Journal of Applied Polymer Science

The Pyrolysis Behaviors of Ternary Copolyimide Derived from Aromatic Dianhydride and Aromatic Diisocyanates

Binghua Guo,[1] Lei Chen,[1] Junrong Yu,[1] Jing Zhu,[1] Guizhen Wang,[2] Zuming Hu[1]

[1]State Key Laboratory of Modification for Chemical Fibers and Polymer Materials, College of Material Science and Engineering, Donghua University, Shanghai 201620, People's Republic of China

[2]Department of Automotive Engineering, Shandong Labor Vocational and Technical College, Jinan 250022, People's Republic of China

Correspondence to: Zuming Hu (E-mail: hzm@dhu.edu.cn)

ABSTRACT: A polyimide (PI) based on benzophenone-3,3′,4,4′-tetracarboxylic acid dianhydride, toluene diisocyanate (TDI), and 4,4′-methylenebis (phenyl isocyanate) (MDI) has been synthesized via a one-step polycondensation procedure. The resulting PI possessed excellent thermal stability with the glass transition temperature (T_g) 316°C, the 5% weight loss temperature ($T_{5\%}$) in air and nitrogen 440.4°C and 448.0°C, respectively. The pyrolysis behaviors were investigated with dynamic thermogravimetric analysis (TGA), TGA coupled with Fourier transform infrared spectrometry (TGA–FTIR) and TGA coupled with mass spectrometry (TGA–MS) under air atmosphere. The results of TGA–FTIR and TGA–MS indicated that the main decomposition products were carbon dioxide (CO_2), carbonic oxide (CO), water (H_2O), ammonia (NH_3), nitric oxide (NO), hydrogen cyanide (HCN), benzene (C_6H_6), and compounds containing NH_2, C≡N, N═C═O or phenyl groups. The activation energy (E_a) of the solid-state process was estimated using Ozawa–Flynn–Wall (OFW) method which resulted to be 143.8 and 87.8 kJ/mol for the first and second stage. The pre-exponential factor (A) and empirical order of decomposition (n) were determined by Friedman method. The activation energies of different mechanism models were calculated from Coats–Redfern method. Compared with the activation energy values obtained from the OFW method, the actual reaction followed a random nucleation mechanism with the integral form $g(\alpha) = -\ln(1-\alpha)$. © 2013 Wiley Periodicals, Inc. J. Appl. Polym. Sci. **2014**, *131*, 40165.

KEYWORDS: degradation; kinetics; polyimides

Received 19 April 2013; accepted 7 November 2013
DOI: 10.1002/app.40165

INTRODUCTION

Aromatic polyimide (PI) has received considerable attention for its potential application in aerospace, microelectronics, optoelectronics, composites, and so on due to its low dielectric constant, excellent dimensional stability, strong solvent resistance, and outstanding thermal and mechanical properties.[1–6] Since the Kapton® PI films were commercialized by DuPont in the early 1960s, a number of aromatic PIs have been reported.[6–10] Another significant PI product is P84® fiber which is famous for its clover-leaf structure of cross section and excellent thermal properties.[11] As we know, the long-term service temperature of P84® fiber is higher than 200°C, and 5% weight loss temperature ($T_{5\%}$) is over 400°C in air. However, to our best knowledge, few articles have studied on both the thermal behaviors and the emissions of volatile organic compounds at increasing temperature under air environment.

It is reported that thermogravimetric analysis (TGA) has been used to estimate the kinetic parameters of degradation processes using Ozawa–Flynn–Wall (OFW) method, Friedman method, Coats–Redfern method, Kissinger method, Criado method,[12,13] and so on. Some researchers have studied degradation mechanism under nitrogen or air atmosphere for PI,[14–17] PI contained phosphorus,[18] silicon,[19] benzobisoxazole,[20] naphthalimide,[21] and blended PI, such as polysulfone/PI,[22] poly(imide-siloxanes),[23] PI/SiO_2,[24] etc.

In this study, a PI based on benzophenone-3,3′,4,4′-tetracarboxylic acid dianhydride (BTDA), toluene diisocyanate (TDI), and 4,4′-methylenebis (phenyl isocyanate) (MDI) has been synthesized via a one-step polycondensation procedure. Chemical structure of the resultant ternary copolyimide was investigated using Fourier transform infrared spectrometry (FTIR) and nuclear magnetic resonance spectroscopy (^{1}H NMR). Also, the pyrolysis behaviors were investigated with dynamic TGA, TGA coupled with Fourier transform infrared spectrometry (TGA–FTIR) and TGA coupled with mass spectrometry (TGA–MS) instruments under air atmosphere. In addition, activation energies (E_a) for thermal degradation were calculated by OFW method; empirical

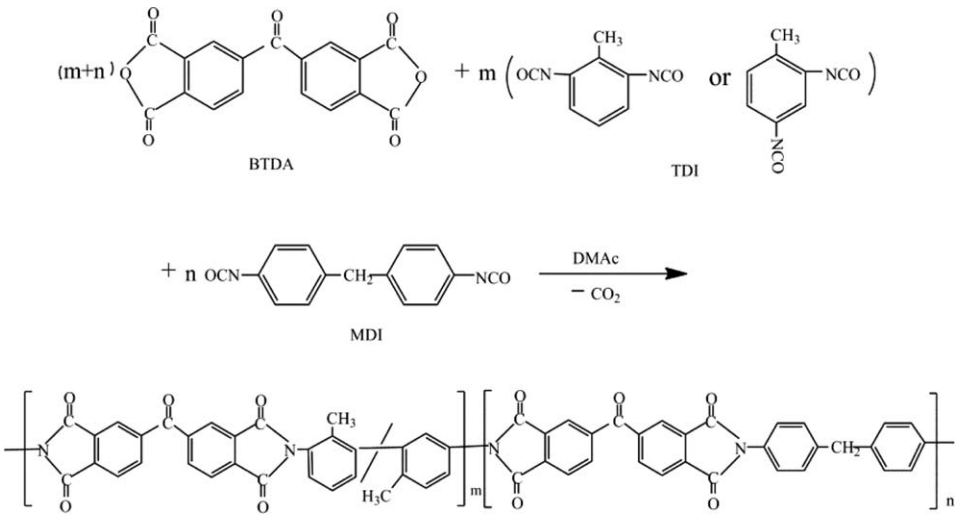

Scheme 1. Synthetic scheme of BTDA–TDI/MDI ternary copolyimide.

order of decomposition (n) and pre-exponential factor (A) were defined using Friedman method; the mechanism of solid-state process was investigated by Coats–Redfern method.

EXPERIMENTAL

Materials

BTDA was purchased from J&K Chemical (Shanghai China) and dried in vacuum oven at 100°C for at least 12 h before use. TDI (mixture of 2,4-isomer [80%] and 2,6-isomer [20%]) was received from Sinopharm Chemical Reagent Co., Ltd. (Shanghai China) and MDI was purchased from Sigma-Aldrich Co. LLC. (Shanghai China). Sodium hydroxide (NaOH) and acetone were obtained from LingFeng Chemicals Co., Ltd. (Shanghai China). The above all chemicals were used as received. *N,N*-dimethylacetamide (DMAc) was obtained from LingFeng Chemicals Co., Ltd. (Shanghai China) and then stored over 4 Å molecular sieves for at least 1 week. Distilled water was self-made.

Measurements

FTIR spectrum of obtained PI was carried out on a Nicolet Nexus 670 spectrometer with an attenuated total reflection (ATR) accessory. ^{1}H NMR spectrum was run on a Bruker AV 400 FT-NMR spectrometer at 400 MHz using deuterated dimethyl sulfoxide (DMSO-*d6*) served as the solvent and tetramethylsilane as the internal reference. Differential scanning calorimetry (DSC) was performed on a TA DSC Q20 at a scan rate of 10°C min^{-1} in flowing nitrogen. TGA was conducted with a Netzsch TG 209 F1 Iris carrying out on approximately 10 mg samples at a heating rate of 10°C min^{-1} under air atmosphere. The TGA–FTIR measurement was carried out in Netzsch TG 209 F1 Iris coupled to a thermo Nicolet 8700 FTIR spectrometer at a heating rate of 10°C min^{-1} with the flow rate of air in the cell 20 mL/min, and both IR cell and transfer line were maintained at 200°C. TGA-MS characterization was performed on a Netzsch STA 449C-Balzers MID instrument. TGA was performed at a scan rate of 10°C min^{-1} in high purity air with a flow rate of 12 mL/min. The connection between TGA and MS was also maintained at 200°C. Inherent viscosity was measured in DMAc at a concentration of 0.5 g/dL at 30°C using a Ubbelohde viscosimeter.

Synthesis of BTDA–TDI/MDI Ternary Copolyimide

The PI was derived from BTDA, TDI, and MDI via a one-step polycondensation and the procedure was given as shown in Scheme 1. A four-necked round bottomed flask equipped with a mechanical stirrer, a nitrogen-inlet and a nitrogen-outlet was charged with a mixture of 16.1 g BTDA (0.05 mol), 0.04 g NaOH (dissolved in water), and 50 mL DMAc. When the mixture was heated to 80°C, isocyanate mixture consisting of 6.96 g TDI and 2.5 g MDI (total molar amount 0.05 mol) was added into the solution dropwise under nitrogen atmosphere. After finishing addition of isocyanate, the reaction continued until completion of CO_2 development at 80°C. With addition of acetone, the obtained PI was precipitated, washed, and then dried. And inherent viscosity of the resulting PI was 0.7950 dL g^{-1}.

RESULTS AND DISCUSSION

Chemical Structure of BTDA–TDI/MDI Ternary Copolyimide

The chemical structure of BTDA–TDI/MDI ternary copolyimide was characterized by FTIR spectrum as shown in Figure 1. The characteristic imide moiety absorption at around 1364 cm^{-1} due to C—N (stretching vibrations) which is newly formed in the copolymer backbone. The other characteristic absorbance peaks observed at around 1780 cm^{-1} (asymmetrical stretch), 1724 cm^{-1}

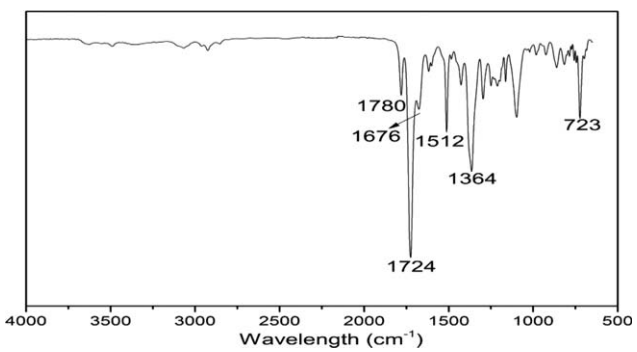

Figure 1. The FTIR spectrum of BTDA–TDI/MDI ternary copolyimide.

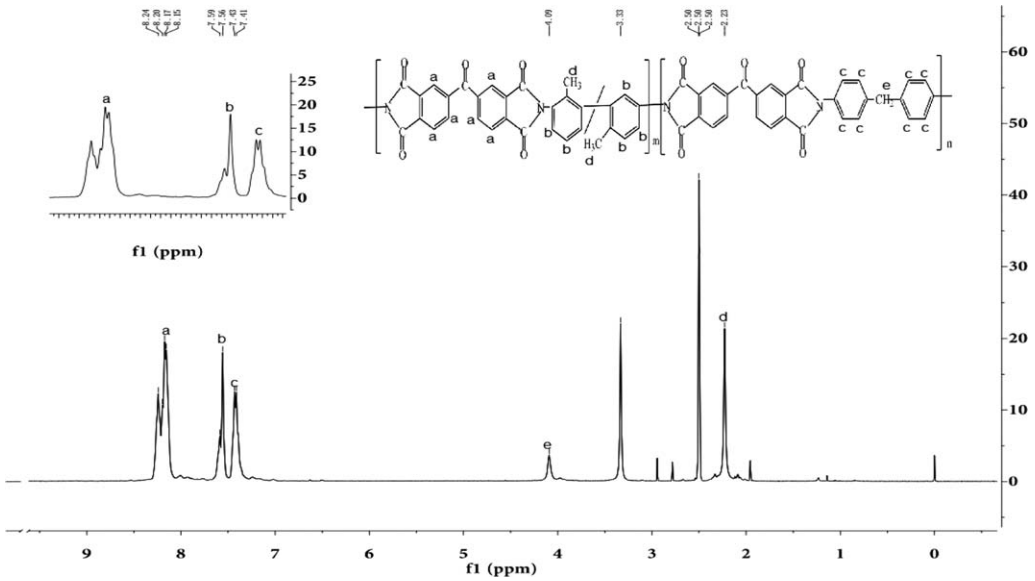

Figure 2. The ^{1}H NMR spectrum of BTDA–TDI/MDI ternary copolyimide.

(symmetrical stretch), and 723 cm^{-1} (flexural vibrations) are assigned to C═O in imide rings, respectively. Meanwhile, the typical absorption peak of C═O belong to ketone moiety is revealed at 1676 cm^{-1} and the strong absorption band corresponding to benzene ring is observed at 1512 cm^{-1}.[25,26] What deserves to be mentioned is that the weak absorption band at 2816–3157 cm^{-1} (stretch vibrations) and 3460–3700 cm^{-1} (stretch vibrations) are assigned to C─H and O─H, respectively. However, absorptions of N─H (3428, 3365, and 1543 cm^{-1}) reported in these literature[27–30] is invisible indicating that there is no amide acid group in the skeleton structure of the polymer. Also, no characteristic peaks of N═C═O and O═C─O belong to isocynate and anhydride are found at 2267 and 1810–1840 cm^{-1}.[31] The fact, to some extent, can demonstrate that almost all monomers have been involved in the reaction.

The chemical structure was further confirmed by ^{1}H NMR spectra displayed in Figure 2 and the chemical shift values of characteristic peaks of monomers BTDA, TDI, and MDI were given as follows: BTDA: ^{1}H NMR (400 MHz, DMSO), ppm δ 8.37–8.20 (m, 2H), 8.08–7.51 (m, 2H), 8.08–7.77 (m, 2H). TDI: ^{1}H NMR (400 MHz, DMSO), ppm δ 7.34–6.94 (m, 3H), 2.23 (d, J = 11.8 Hz, 3H). MDI: ^{1}H NMR (400 MHz, DMSO), ppm δ 7.43–7.07 (m, 8H), 3.88 (d, J = 21.6 Hz, 2H).

The protons (H_a, H_b, and H_c) adjacent to the aromatic rings resonated at downfield region around 8.2, 7.6, and 7.4 ppm in the spectrum due to the phenyl groups originating from BTDA, TDI, and MDI, respectively. The protons of CH_2 groups (H_e) displayed at 4.1 ppm shift downfield which is 3.88 ppm in ^{1}H NMR spectrum of MDI. The single signal of H_d at 2.2 ppm is assignable to CH_3 which appears at a higher field because it is less affected by other protons. Compared with the chemical shift values of monomers, the variations suggest that all the monomers were involved in reaction leading to the chemical environment of protons changed. Here, it is worth mentioning that signals of DMSO-*d*6 and water in DMSO solvent are observed at 2.5 and 3.4 ppm.

Thermal Properties of BTDA–TDI/MDI Ternary Copolyimide

The thermal properties of PI copolymer were evaluated by glass transition temperature (T_g) and decomposition temperature (T_d) determined by DSC and TGA, respectively.

Differential Scanning Calorimetry (DSC). Glass transition temperature of BTDA–TDI/MDI ternary copolyimide was determined by means of DSC during the second heating process from 50°C to 400°C with a heating rate of 10°C min^{-1} under nitrogen. As shown in Figure 3, a strong endothermic peak relating to T_g is observed at 316°C.

Thermogravimetric Analysis (TGA). Thermal stability and thermo-oxidative degradation behaviors of ternary copolyimide were studied by determining its mass loss during heating. The mass loss (TG%) and derivative mass loss (DTG) curves are presented in Figure 4. As can be observed, the PI shows excellent thermal stability under both air and nitrogen environments. Meanwhile, it is clear from Table I that both 5% weight loss temperature ($T_{5\%}$) and 10% weight loss temperature ($T_{10\%}$) in

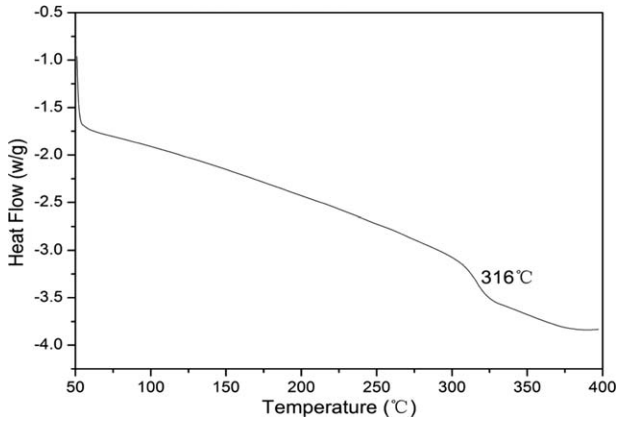

Figure 3. The DSC thermogram of BTDA–TDI/MDI ternary copolyimide in nitrogen.

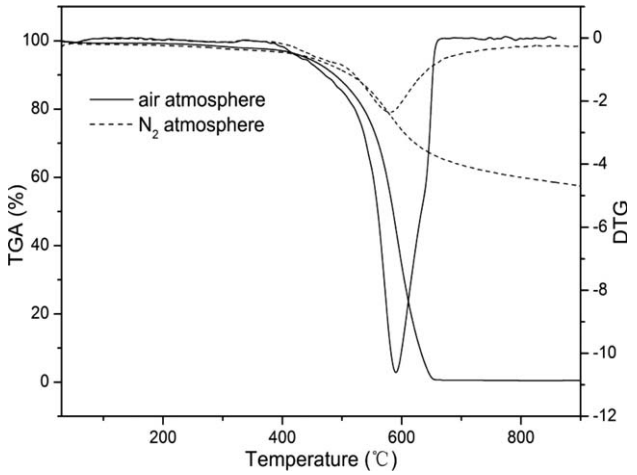

Figure 4. Thermal degradation of BTDA–TDI/MDI ternary copolyimide, weight loss (TG), and derivative mass loss (DTG) versus temperature with heating rate 10°C min^{-1}.

nitrogen are higher than in air at the same heating rate. Therefore, thermal stability in nitrogen is a little better than in air. In addition, comparing with nitrogen atmosphere, almost no char residue is left in air. The phenomenon illustrated that these PIs could be oxidized to polymer peroxide or phenyl radical by oxygen more easily in air.[32] In addition, it is noteworthy that a single-stage decomposition is found both under air and nitrogen atmospheres with a remarkable weight decrease in a narrow temperature range and the highest decomposition rate at around 590.4°C and 580.5°C, respectively. The results are different from the similar PI synthesized from aromatic dianhydride with isocyanate[33] or dianiline[34] which began to decompose below 400°C and showed an obvious two-stage degradation process throughout the decomposition. Generally, the two-stage degradation process is usually assigned to the cleavage of small molecules from long flexible segments at moderate temperature and then the breakage of rigid imide and benzene rings at higher temperature. However, for our PIs, it seems that the thermal stability is not destroyed by the flexible —CH_2— and —CH_3— groups contained in the polymer with the $T_{5\%}$ 440.4°C and 448.0°C in air and nitrogen atmospheres, respectively. And the excellent thermal stability was primarily due to the thermostable imide groups and benzene rings in the main chain.

Table I. Thermal Properties of Polyimide in Air and Nitrogen Atmospheres

Atmosphere	$T_{5\%}$[a] (°C)	$T_{10\%}$[b] (°C)	T_{max}[c] (°C)	Char yield[d] (%)
Air	440.4	487.8	590.4	0.56
Nitrogen	448.0	514.0	580.5	57.5

[a] A 5% weight loss temperature was detected at a heating rate of 10°C min^{-1} with a gas flow of 20 mL min^{-1}.
[b] A 10% weight loss temperature was detected at a heating rate of 10°C min^{-1} with a gas flow of 20 mL min^{-1}.
[c] The temperature of maximum degradation rate.
[d] Residual weight percentage at 900°C.

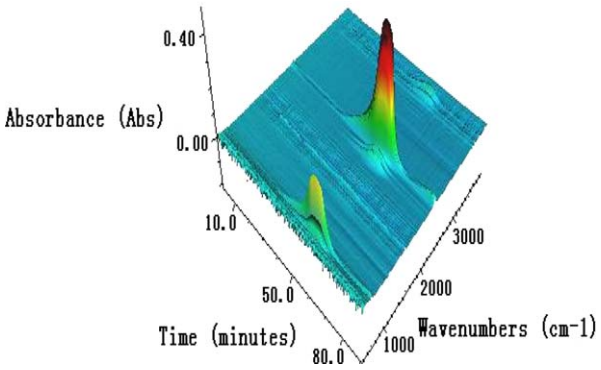

Figure 5. The three-dimensional spectra of evolved compounds at different times for BTDA–TDI/MDI ternary copolyimide. [Color figure can be viewed in the online issue, which is available at wileyonlinelibrary.com.]

TGA–FTIR Characterization of Volatile Products. The TGA–FTIR instrument was applied in order to obtain information about the evolved compounds of BTDA–TDI/MDI ternary copolyimide at different times during the thermogravimetric experiment. The spectra data of released gaseous products were collected in the form of interferograms continuously. As can be seen from Figure 5, the absorbances of evolved compounds were firstly detected at about 400°C which is coincident with the initial decomposition temperature displayed in TGA thermogram (shown in Figure 4 and Table I). Additionally, the characteristic bands of evolved volatile products mainly exhibiting in the range of 3500–4000 cm^{-1}, 2000–2500 cm^{-1}, 1600–1200 cm^{-1}, and 500–1000 cm^{-1} fit well to the reported FTIR features of volatile products such as CO_2 (2300–2400 cm^{-1}), CO (2250–2300 cm^{-1}), benzene (1450–1600 cm^{-1}), and H_2O (3400–4000 cm^{-1}).[31,35,36] Moreover, Figure 5 shows us that remarkable difference occurs after 390°C with the absorbance intensity getting stronger and stronger up to 700°C and then becoming weak. The fact, on one hand, might be as a result of accumulative effect as the same product was getting together in the acceptor making its density greater than actual one; on the other hand, might be due to the delay when the evolved products were transferred from TGA to FTIR apparatus by the flow of nitrogen.

Since there was almost no residue left after heating to 900°C under air environment, we have ample reasons to assume that all samples turned to gaseous products with the action of oxidation and high temperature and escaped from the TGA furnace. That is because the oxygen in air could react with not only PI to polymer peroxide or phenyl radical but primary decomposition products to CO, CO_2, H_2O, and so on.[36–38] A stacked plot of the IR spectra of gaseous species from TGA instrument under air are displayed in Figure 6. Absorption bands registered in the range of 3500–4000 cm^{-1} correspond to stretching vibrations of products containing hydrogenous groups, such as C—H, O—H, and the most possible escaped compounds are H_2O.[35,36,38] The spectral characteristics are the bands at 2364 and 671 cm^{-1}, due to the stretching and flexural vibrations of C═O, respectively. And the corresponding products might be CO_2 which is especially noticeable from the IR bands. The broad band at 2310 cm^{-1} is assigned to asymmetric stretching

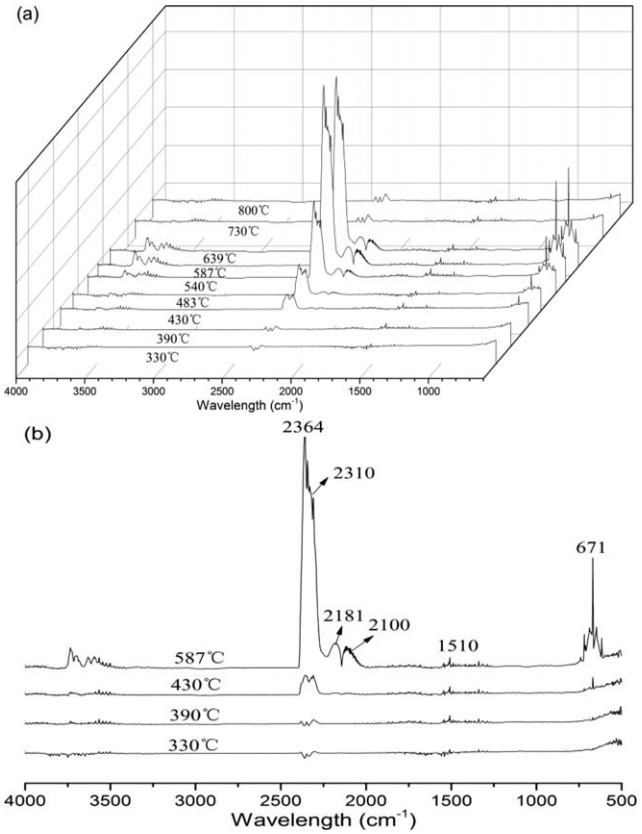

Figure 6. FTIR spectra of the evolved compounds at different times for BTDA–TDI/MDI ternary copolyimide.

vibrations of N═C═O[15,31] which overlaps the absorption peaks of CO_2 mainly because of the similar chemical structure. The double absorption at the right side of CO_2 (2181 and 2100 cm^{-1}) might due to the released CO gas which was detectable at 480°C for the first time. Also, the weak absorption at around 1500–1650 cm^{-1} might be due to the evolution of unsaturated aromatic hydrocarbons indicating the existence of benzene ring. At the same time, the weak absorbance bands in the range of 1200–1400 cm^{-1} might assign to symmetrical stretch vibrations of oxynitride, such as NO.[31] It is noted that the possible absorbance bands of compounds containing element nitrogen are unconspicuous and easy to be neglected in the IR spectra. Therefore, more evidences are needed to identify where the element nitrogen goes.

TGA–MS Characterization of Volatile Products. The degradation process of BTDA–TDI/MDI ternary copolyimide was further studied by TGA–MS analysis to provide deeper insight into pyrolysis behavior. And the detailed results (presented in Figure 7) are displayed in the form of ion current intensity versus temperature for the evolved products. In comparison with TGA–FTIR (Figure 6) and TGA–MS (Figure 7), the results showed good repeatability which could help us to understand the pyrolysis behaviors better. It can be observed from Figure 7 that intensive signals of the products with different mass to charge ratios (*m/z*) appear within the temperature range of 500°C–650°C except that the weak peak of *m/z* 18 also appears at 80°C–150°C. This temperature range is a little higher than that of the degradation stage

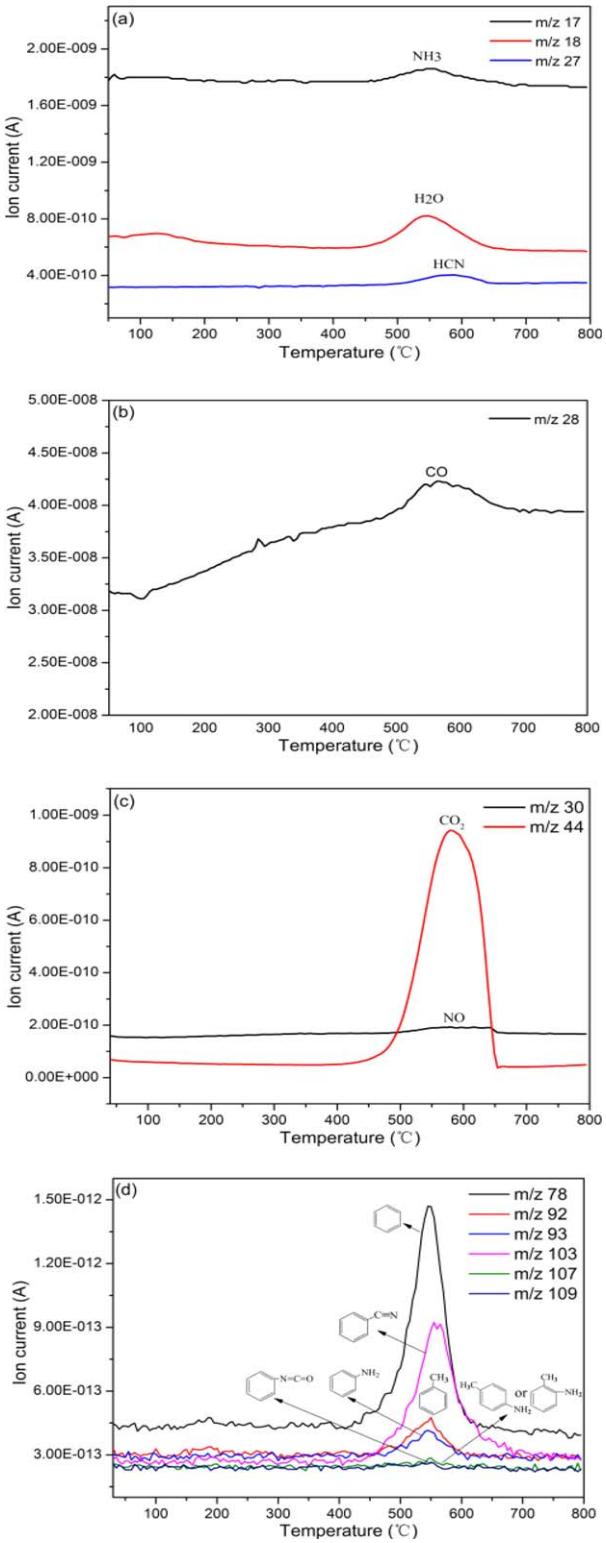

Figure 7. Single ion current for the fragments generated from thermal degradation of BTDA–TDI/MDI ternary copolyimide: (**a**) *m/z* = 17, 18, and 27; (**b**) *m/z* = 28; (**c**) *m/z* = 30 and 44; (**d**) *m/z* = 78, 92, 93, 103, 107, and 109. [Color figure can be viewed in the online issue, which is available at wileyonlinelibrary.com.]

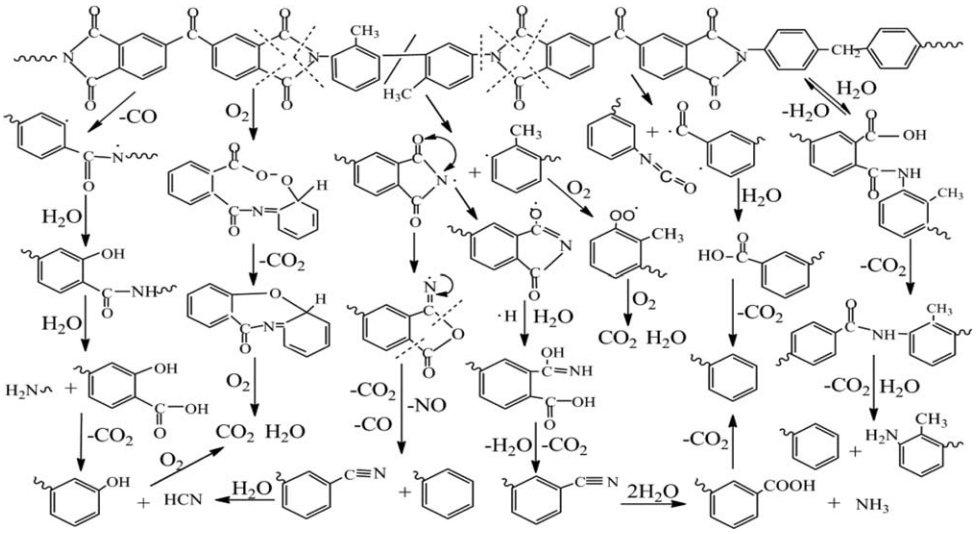

Scheme 2. The possible decomposition mechanism of BTDA–TDI/MDI ternary copolyimide in air.

described in Figure 4 which might be due to the delay between sample degradation and mass spectroscopy. According to TGA–MS analysis, the mass to charge ratios *m/z* 17, 27, and 30 correspond to fragments ammonia (NH_3), hydrogen cyanide (HCN), and nitric oxide (NO), respectively, which are absent or unobvious in IR spectra. It is noted that the light volatile nitrogenous species evolve mainly in the form of NH_3, HCN, and NO during pyrolysis. However, some authors[39] also believed that nitrogenous species, such as NH_3 and HCN, might undergo further reduction or oxidation to N_2 or NO depending on the extent of the limited availability of O_2 within the pyrolysing process. Water (H_2O) can be confirmed by *m/z* 18. It turns out that there are two steps for water generation, the first step is seen very early at 80°C–150°C due to the residual water evaporating from the sample[40]; the second one occurs around 500°C originating from the degradation of polymer. However, water escaping from the sample at the first step could accelerate pyrolysis of PI for resulting in cleavage and decarboxylation of imide rings with the help of high temperature.[41] An increase of signal assigned to carbon oxide (CO, *m/z* 28) is detected until at a very high temperature (above 600°C) with the greatest ion current intensity. The phenomenon could be explained by the fact that the generation of CO is through the release of the carbonyl groups by breaking C—N and C—C bonds of imide rings[42] which is continuous during the whole heating process. Carbon dioxide (CO_2) fragments can be determined by *m/z* 44.[43–45] As depicted in Figure 7(c), CO_2 is barely detectable until 430°C and the intensity of ion current reaches the maximum value at about 580°C. All results are coincident with the FTIR results. Generally, the generation of CO_2 is through the pyrolytic cleavage and decarboxylation of the carboxylic acid groups.[39] Also, fragments of *m/z* 78, 92, and 93 belong to benzene, toluene, and aniline[44]; benzonitrile (*m/z* 103), aminotoluene (*m/z* 107), and benzene-diisocyanate (*m/z* 109) can also be identified as shown in Figure 7(d). These data are not in good agreement with the earlier observation by Shen et al.[15] and Stephen et al.[42] since the volatile products they detected from the FTIR results are CO, CO_2, H_2O and CO, CO_2, respectively. However, our results support the fact that the gaseous products are CO, CO_2, H_2O, NH_3, NO, HCN, benzene, and compounds containing NH_2, C≡N, N═C═O, or phenyl groups.

The volatile species obtained from measurements of TGA–FTIR and TGA–MS could be used to propose the pyrolysis behaviors of BTDA–TDI/MDI ternary copolyimide. And the possible decomposition mechanism[15] is illustrated as Scheme 2.

Degradation Kinetic Analysis

Theoretical Background. In general, the decomposition of solid polymer can be associated with the reactions which may be represented by the process

$$A_{solid} \rightarrow B_{solid} + C_{gas} \quad (1)$$

where A is the initial, B is the residue, and C is the gas. For TGA, the degree of decomposition can be calculated as follows:

$$\alpha = \frac{(W_o - W_t)}{(W_o - W_i)} \quad (2)$$

where W_o is the initial mass of the sample, W_t is the residual mass at time t, and W_i is the residual mass at infinite time, α is the fractional extent of reaction.

All kinetic calculations assume that the isothermal rate of conversion is a linear function of a constant which is temperature-dependent and a temperature-independent function of the conversion α, and it can be expressed as:

$$\frac{d\alpha}{dt} = kf(\alpha) \quad (3)$$

where $\frac{d\alpha}{dt}$ is the rate of conversion, k is the decomposition rate constant, depending on temperature in an Arrhenius form, $f(\alpha)$ expresses a kinetic model function of the conversion of reactive group which depends on the particular decomposition mechanism. According to the Arrhenius equation,

$$k = A \exp(-E_a/RT) \quad (4)$$

where A, the pre-exponential factor (s^{-1}), is assumed to be independent of temperature, E_a is the activation energy

Table II. Algebraic Expressions for $g(\alpha)$ for the Mechanisms of Solid-State Processes

Symbol	$g(\alpha)$	Solid-state processes
Sigmoidal curves		
A_2	$[-\ln(1-\alpha)]^2$	Nucleation and growth (Avrami equation 1)
A_3	$[-\ln(1-\alpha)]^3$	Nucleation and growth (Avrami equation 2)
A_4	$[-\ln(1-\alpha)]^4$	Nucleation and growth (Avrami equation 3)
Deceleration curves		
R_1	α	Phase boundary controlled reaction (one-dimensional movement)
R_2	$2[1-\ln(1-\alpha)^{1/2}]$	Phase boundary controlled reaction (contracting area)
R_3	$3[1-\ln(1-\alpha)^{1/3}]$	Phase boundary controlled reaction (contracting volume)
D_1	α^2	One-dimensional diffusion
D_2	$(1-\alpha)\ln(1-\alpha)+\alpha$	Two-dimensional diffusion (Valensi equation)
D_3	$[1-(1-\alpha)^{1/3}]^2$	Three-dimensional diffusion (Jander equation)
D_4	$[1-(2/3)\alpha]-(1-\alpha)^{2/3}$	Three-dimensional diffusion (Ginstling–Brounshtein equation)
F_1	$-\ln(1-\alpha)$	Random nucleation with one nucleus on the individual particle
F_2	$1/(1-\alpha)$	Random nucleation with two nuclei on the individual particle
F_3	$1/(1-\alpha)^2$	Random nucleation with three nuclei on the individual particle

(kJ/mol), T is the absolute temperature (K), and R is the gas constant (8.314 J/mol K). Combining eqs. (3) and (4) gives

$$\frac{d\alpha}{dt}=A\ \exp\left(-E_a/RT\right)\ f(\alpha) \tag{5}$$

For non-isothermal measurements at controlled and constant heating rate$\beta\left(\beta=\frac{dT}{dt}\right)$, eq. (5) can be transformed to

$$\frac{d\alpha}{dT}=\frac{A}{\beta}\exp\left(-E_a/RT\right)f(\alpha) \tag{6}$$

Therefore, eq. (6) is the fundamental relation to determine kinetic parameters on the basis of TGA data.

Ozawa–Flynn–Wall Method. The OFW method,[13,46] is a isoconversional and "model-free" method which assumes that the conversion function $f(\alpha)$ does not change with the alteration of the heating rate for all values of α. It is one of the integral methods that can determine the activation energy without a precise knowledge of reaction mechanism. It involves the measuring of the temperature corresponding to fixed values of α from experiments at different heating rates β. Integration of eq. (6) from an initial temperature T_0, where the degree of conversion is $\alpha = \alpha_0$, to the peak temperature T_p, corresponding to $\alpha = \alpha_p$, gives

$$g(\alpha)=\int_{\alpha_0}^{\alpha_p}\frac{d\alpha}{f(\alpha)}=\frac{A}{\beta}\int_{T_0}^{T_p}\exp\left(-E_a/RT\right)dT \tag{7}$$

suggesting $x = E/RT$, $g(\alpha)$ is the function of conversion. The eq. (7) can be expressed as

$$\frac{A}{\beta}\int_{T_0}^{T_p}\exp\left(-E_a/RT\right)dT=\frac{AE_a}{\beta T}p(x) \tag{8}$$

Taking logarithms, gives

$$\log\beta=\log\frac{AE_a}{g(\alpha)R}+\ \log p(x) \tag{9}$$

where

$$p(x)=\frac{e^{-x}}{x^2}\sum_{n=1}(-1)^{n-1}(n!/x^{n-1})$$

Using the Doyle's approximation, if $20\leq x\leq 60$, the function $p(x)$ can be written as the following approximation:

$$\log p(x)\approx -2.315-0.4567x \tag{10}$$

substituting eq. (10) to eq. (9), it can be obtained:

$$\log\beta=\ \log\frac{AE_a}{g(\alpha)R}-2.315-\frac{0.4567E_a}{RT} \tag{11}$$

Plotting $\log(\beta)$ against $1/T$ according to eq. (11) for a fixed degree of decomposition, the apparent activation energy (E_a) can be obtained.

Friedman Method. Friedman method[47,48] is also a isoconversional method which is based on eq. (3) and Arrhenius eq. (4). It proposes to apply the logarithm of the conversion rate $\frac{d\alpha}{dt}$ as a function of the reciprocal temperature. The eq. (7) transforms to

$$\ln\left[\beta\left(\frac{d\alpha}{dT}\right)\right]\ =\ln A+n\ln\left(1-\alpha\right)-E_a/RT \tag{12}$$

by plotting $\ln\left[\beta\left(\frac{d\alpha}{dT}\right)\right]$ against $1/T$, the value of $-E_a/R$ for a given α can be obtained directly.

Coats–Redfern Method. The Coats–Redfern method[49] uses an asymptotic approximation for the resolution of eq. (7) at different conversion values. If $(2RT)/E_a \rightarrow 0$ is true for the Doyle approximation, a natural logarithmic form can be obtained:

$$\ln\frac{g(\alpha)}{T^2}=\ln\frac{AR}{\beta E}-\frac{E_a}{RT} \tag{13}$$

according to the different degradation processes, with the theoretical function $g(\alpha)$ being listed in Table II, E_a and A can be determined from a plot of $\ln\frac{g(\alpha)}{T^2}$ versus $1000/T$, as well as the valid reaction mechanism.

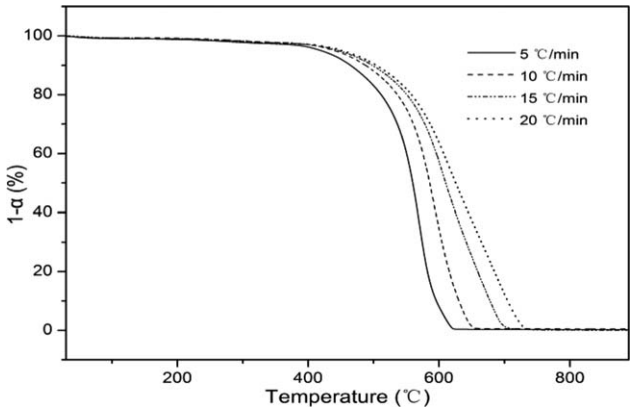

Figure 8. The TGA curves at different heating rates.

The Determination of Activation Energies. The thermal degradation curves and DTG curves carried out at different heating rates are shown in Figures 8 and 9. Obviously, the onset decomposition temperature increases with the increase of heating rate. The activation energy (E_a) of thermal degradation for copolyimide could be obtained by the OFW method from a linear fitting of logβ versus 1000/T at a fixed conversion with the slope of $-0.4567E_a/RT$. For our study, the conversion values are 0.05, 0.10, 0.20, 0.30, 0.40, 0.50, 0.60, 0.70, 0.80, 0.90, and 0.95. The fitting straight lines are showed in Figure 10 and the corresponding activation energies calculated from the slopes are displayed in Figure 11. All of the fitting lines are nearly parallel indicating that the OFW method is applicable to our system. From the results depicted in Figure 11, we can see that the calculated activation energies decrease with the increase of conversional degrees and there seems to be three energy barriers during the whole decomposition process. The first energy barrier happened when the conversional degree was smaller than 0.20, the second one appeared when the conversional degree was between 0.20 and 0.40, the last one turned up when the conversional degree was larger than 0.80. It seems that the degradation process could be divided into two phases by the conversion degree 0.50 as the average activation energies for the first phase (143.8 kJ/mol) are much higher than the second one (87.8 kJ/mol). However, the result is inconsistent with the one-stage degradation process (shown in Figures 4 and 8). On the other hand, observed from DTG curves in Figure 9, another weak peak appears when the conversion degree value is about 0.90 suggesting rapid decomposition. And it becomes visible as the heating rates increases. In other words, it is not strict one-stage degradation as a result of hysteresis of heat transmission making the PI fragments disintegrate at a higher temperature. In addition, it seems that the pyrolysis of copolyimide is more difficult at the first start, and it becomes easier once the main chemical structures are destroyed. The phenomenon might be due to the residue formed during the first step of decomposition, which could further react with oxygen to oxidized products. And these complex products are less stable and require lower activation energy for its degradation.[16]

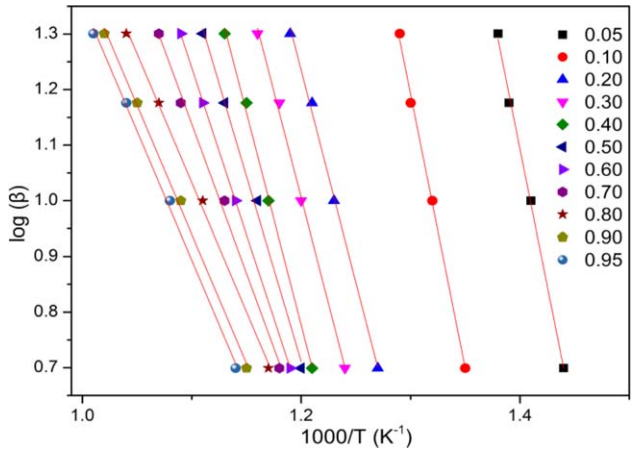

Figure 10. Ozawa–Flynn–Wall plots at varying conversions. [Color figure can be viewed in the online issue, which is available at wileyonlinelibrary.com.]

On the other hand, the E_a of two stages is much lower than the dissociation energy of C—N bond (305 kJ/mol), the weakest bond of the polymers. Hence, the decomposition of the resultant PI could be mainly governed by the molecular structure and kinetic consideration not by energy of bond breaking.[19] Similar results were observed in literatures[14,15] which also revealed that the calculated activation energy was lower than the weakest bond dissociation energy, indicating similar degradation mechanism. Furthermore, the activation energy decreases sharply when the conversional degree value is in the range of 0.40–0.80, saying, the temperature is between 575°C and 616°C ($\beta = 10$°C

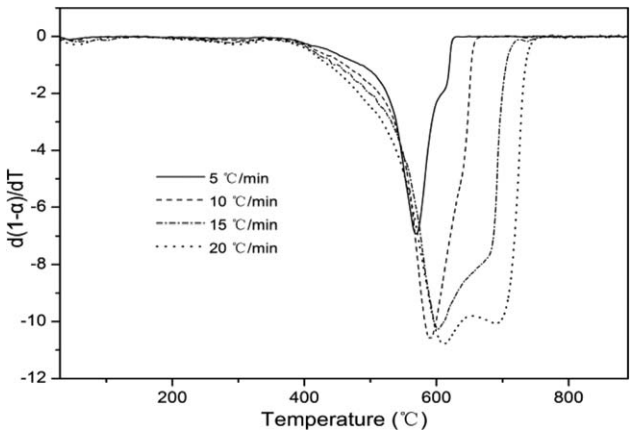

Figure 9. The DTG curves at different heating rates.

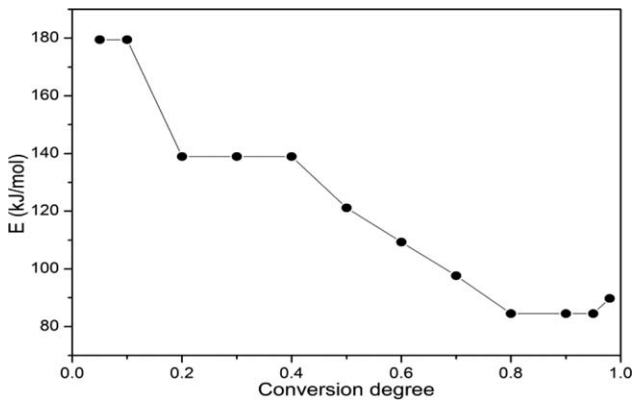

Figure 11. Activation energies obtained by Ozawa–Flynn–Wall method.

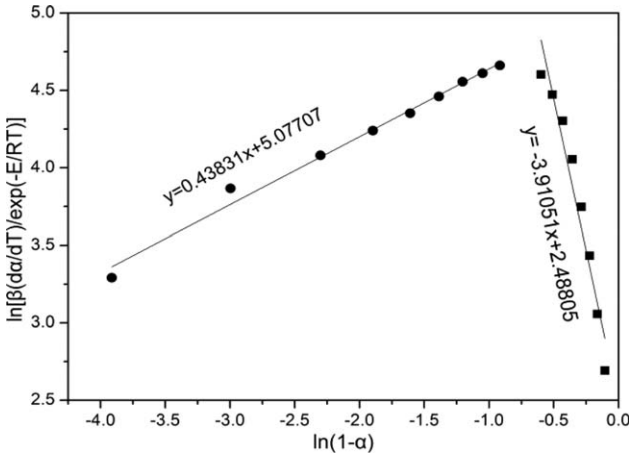

Figure 12. The empirical order of decomposition and the pre-exponential factor from Friedman calculation.

min^{-1}), which is consistent with the temperature range 550°C–654°C shown in Figure 4 quite well with the maximum decomposition rate 590.4°C.

Determination of Kinetic Mechanism. Generally, the conversion functional relationship $f(\alpha)$ is defined to the proportional to the mass quotient of the unreacted material[50]:

$$f(\alpha) = (1-\alpha)^n \quad (14)$$

where n is the reaction order. Combining eqs. (8) and (6) leads to

$$\ln[\beta(d\alpha/dT)/\exp(-E_a/RT)] = \ln A + n\ln(1-\alpha) \quad (15)$$

The activation energy of PI was obtained from linear plotting of $\ln(1-\alpha)$ against $\ln[\beta(d\alpha/dT)/\exp(-E_a/RT)]$ at a fixed conversion with the slope of being n and the intercept being $\ln A$.[51] As shown in Figure 12, the empirical order of decomposition (n) and the pre-exponential factor (A) were different from each other when the conversion degrees were varying from 0.05 to 0.95. The calculated n and A were −3.9 and 12.1 s^{-1}, respectively when the conversion degrees were under 0.5 while the values were 0.4 and 160.8 s^{-1}, respectively, when the conversion degrees were above 0.5. The fact indicates that the decomposition process of BTDA–TDI/MDI ternary copolyimide was complicated. And there might be two stages during the thermal degradation which is in good agreement with the results from activation energy.

According to eq. (13), activation energy for every $g(\alpha)$ listed in Table II[16] can be obtained from a linear fitting of $\ln[(g(\alpha)/T^2]$ versus $1000/T$ at a constant heating rate and different conversions using the Coats–Redfern method. The same conversion degree values were used just as in OFW method. The activation energies and correlations for the first and second stage are tabulated in Table III for different conversions in the range of 0.05–0.95 at a heating rate of 10°C min^{-1}. For the first stage, Table III shows that the correlation coefficients of R_1, R_2, R_3, D_1, D_2, F_2, and F_3 are bad, so these degradation mechanisms were excluded first. In addition, comparing with the calculated values of activation energies in Table III, the activation energy (157.9 kJ/mol) is in better agreement with that obtained from OFW method (143.8 kJ/mol), corresponding to F_1 type mechanism $[-\ln(1-\alpha)]$ and the correlation coefficient is good (0.99892). For the second stage, the degradation mechanisms of R_2, R_3, F_2, and F_3 were also excluded because activation energies cannot be obtained from the slope of corresponding linear fitting of $g(\alpha)$. Meanwhile, the calculated activation energy (60.1 kJ/mol) is in better accordance with the value obtained (87.8 kJ/mol), which also corresponds to the mechanism F_1 style and the correlation coefficient is not bad (0.99540). In other words, for both the first and second stages, the probable solid-state thermodegradation kinetic mechanisms followed by BTDA–TDI/MDI ternary copolyimide are identical, which is random nucleation with one nucleus on the individual particle.

Table III. The Activation Energies for Different Mechanisms

	First stage		Second stage	
Mechanisms	Activation energies (kJ/mol)	Correlations	Activation energies (kJ/mol)	Correlations
A_2	330.3	0.99900	132.8	0.99592
A_3	502.6	0.99902	205.5	0.99607
A_4	675.0	0.99904	278.2	0.99614
R_1	79.3	0.94487	55.9	0.99774
R_2	46.3	0.92561	—	—
R_3	32.2	0.89095	—	—
D_1	173.0	0.95386	124.6	0.99794
D_2	211.3	0.97674	127.2	0.99734
D_3	266.9	0.99484	130.0	0.99666
D_4	229.3	0.98494	128.2	0.99712
F_1	157.9	0.99892	60.1	0.99540
F_2	193.1	0.88651	—	—
F_3	400.6	0.89356	—	—

CONCLUSIONS

A PI derived from BTDA, TDI, and MDI was prepared via a one-step method. The resultant ternary copolyimide possessed good thermal property and high T_g. The main evolved products determined by TGA–FTIR and TGA–MS under air atmosphere were CO_2, CO, H_2O, NH_3, NO, HCN, benzene, and compounds containing NH_2, C≡N, N═C═O or phenyl groups. The kinetic parameters of BTDA–TDI/MDI ternary copolyimide were investigated using different methods. The results indicated that there were two stages during the whole thermal degradation process. For the first stage, the activation energy (E_a) obtained by OFW method was 143.8 kJ/mol with the pre-exponential factor (A) and empirical order of decomposition (n) being 12.1 s^{-1} and −3.9, respectively; for the second stage, the corresponding activation energy was 87.8 kJ/mol with the values of A and n being 160.8 s^{-1} and 0.4, respectively. Activation energies calculated from Coats–Redflern method suggested that both the first and second degradation stages followed the same random nucleation mechanism with the integral form $g(\alpha) = -\ln(1-\alpha)$.

REFERENCES

1. Wang, C. Y.; Zhao, X. Y.; Li, G. Jiang, J. M. *Polym. Degrad. Stabil.* **2009**, *94*, 1526–1532.
2. Hajipour, A. R.; Abrishami, F. *J. Appl. Polym. Sci.* **2012**, *124*, 1757–1763.
3. Chao, M.; Kou, K. C.; Wu, G. L.; Zhang, D. N. *J. Macromol. Sci. A* **2012**, *49*, 578–585.
4. Yan, S. Y.; Chen, W. Q.; Yang, X. J.; Chen, C. A.; Huang, M. F.; Xu, Z. S.; Yeung, K. W. K.; Yi, C. F. *Polym. Bull.*, **2011**, *66*, 1191–1206.
5. Shundrina, I. K.; Vaganova, T. A.; Kusov, S. Z.; Rodionov, V. I.; Karpova, E. V. Malykhin, E. V. *J. Fluorine Chem.* **2011**, *132*, 207–215.
6. Zhu, Y. Q.; Zhao, P. Q.; Cai, X. D.; Meng, W. D.; Qing, F. L. *Polymer* **2007**, *48*, 3116–3124.
7. Zhao, X.; Li, Y. F.; Zhang, S. H.; Shao, Y.; Wang, X. L. *Polymer* **2007**, *48*, 5241–5249.
8. Zhao, X. J.; Liu, J. G.; Yang, H. X.; Fan, L.; Yang, S. Y. *Eur. Polym. J.* **2008**, *44*, 808–820.
9. Zolotukhin, M. G.; Rueda, D. R.; Calleja, F. J. B.; Cagiao, M. E.; Bruix, M.; Sedova, E. A.; Gileva, N. G. *Polymer* **1997**, *38*, 1471–1476.
10. Zheng, Y. H.; Zhai, Y.; Li, G. Z.; Guo, B. H.; Zeng, X. M.; Wang, L. C.; Yu, H. Y.; Guo, J. M. *J. Appl. Polym. Sci.* **2011**, *121*, 702–706.
11. Austria *Pat.* 4,801,502, **1987**.
12. Regnier, N.; Guibe, C. *Polym. Degrad. Stabil.* **1997**, *55*, 165–172.
13. Dowdy, D. R. *J. Therm. Anal.* **1987**, *32*, 137–147.
14. Hondred, P. R.; Yoon, S.; Bowler, N.; Moukhina, E.; Kessler, M. R. *High Perform. Polym.* **2011**, *23*, 335–342.
15. Shen, Y. X.; Zhan, M. S.; Wang, K.; Li, X. H.; Pan, P. C. *J. Appl. Polym. Sci.* **2010**, *115*, 1680–1687.
16. Pramoda, K. P.; Chung, T. S.; Liu, S. L.; Oikawa, H.; Yamaguchi, A. *Polym. Degrad. Stabil.* **2000**, *67*, 365–374.
17. Kim, Y. J.; Glass, T. E.; Lyle, G. D.; Mcgrath, J. E. *Macromolecules* **1993**, *26*, 1344–1358.
18. Chang, T. C.; Wu, K. H.; Chiu, Y. S. *Polym. Degrad. Stabil.* **1999**, *63*, 103–109.
19. Tiptipakorn, S.; Damrongsakkul, S.; Ando, S.; Hemvichian, K.; Rimdusit, S. *Polym. Degrad. Stabil.* **2007**, *92*, 1265–1278.
20. Meng, X. L.; Huang, Y. D.; Yu, H.; Lv, Z. S. *Polym. Degrad. Stabil.* **2007**, *92*, 962–967.
21. UrRehman, S.; Li, P.; Zhou, H. W.; Zhao, X. G.; Dang, G. D.; Chen, C. H. *Polym. Degrad. Stabil.* **2012**, *97*, 1581–1588.
22. Rafiq, S.; Man, Z.; Maitra, S.; Muhammad, N.; Ahmad, F. *J. Appl. Polym. Sci.* **2012**, *123*, 3755–3763.
23. Moon, Y. D.; Lee, Y. M. *J. Appl. Polym. Sci.* **1993**, *50*, 1461–1473.
24. Bin Ahmad, M.; Gharayebi, Y.; Salit, M. S.; Hussein, M. Z.; Ebrahimiasl, S.; Dehzangi, A. *Int. J. Mol. Sci.* **2012**, *13*, 4860–4872.
25. Snyder, R. W.; Thomson, B.; Bartges, B.; Czerniawski, D.; Painter, P. C. *Macromolecules* **1989**, *22*, 4166–4172.
26. Pryde, C. A. *J. Polym. Sci. Pol. Chem.* **1989**, *27*, 711–724.
27. Watanabe, Y.; Shibasaki, Y.; Ando, S.; Ueda, M. *Polymer* **2005**, *46*, 5903–5908.
28. Yang, C. P.; Chen, R. S.; Wei, C. S. *Polym. Int.* **2002**, *51*, 1323–1333.
29. Lai, H.; Qin, L.; Liu, X. Y.; Gu, Y. *Eur. Polym. J.* **2008**, *44*, 3724–3731.
30. Wang, H. H.; Wu, S. P. *J. Polym. Res.* **2005**, *12*, 37–47.
31. Erno Pretsch, P. B., Mart in Badertscher, Springer: New York, **2009**; Chapter *7*, pp 301–323.
32. Kuroda, S.; Mita, I. *Eur. Polym. J.* **1989**, *25*, 611–620.
33. Liu, X. Y.; Zhan, M. S.; Wang, K. *High Perform. Polym.* **2012**, *24*, 373–378.
34. Fang, Y. Q.; Wang, J. A.; Zhang, Q.; Zeng, Y.; Wang, Y. H. *Eur. Polym. J.* **2010**, *46*, 1163–1167.
35. Chen, X. L.; Jiao, C. M. *Polym. Degrad. Stabil.* **2008**, *93*, 2222–2225.
36. Aguirresarobe, R. H.;Irusta, L.; Fernandez-Berridi, M. *J. Polym. Degrad. Stabil.* **2012**, *97*, 1671–1679.
37. Zou, H. T.; Yi, C. H.; Wang, L. X.; Liu, H. T.; Xu, W. L. *J. Therm. Anal. Calorim.* **2009**, *97*, 929–935.
38. Chen, X. L.; Zhuo, J. L.; Jiao, C. M. *Polym. Degrad. Stabil.* **2012**, *97*, 2143–2147.
39. Singh, S.; Wu, C. F.; Williams, P. T. *J. Anal. Appl. Pyrol.* **2012**, *94*, 99–107.
40. Hardy, A.; Van Werde, K.; Vanhoyland, G.; Van Bael, M. K.; Mullens, J.; Van Poucke, L. C. *Thermochim. Acta* **2003**, *397*, 143–153.
41. Chou, W. J.; Wang, C. C.; Chen, C. Y. *Polym. Degrad. Stabil.* **2008**, *93*, 745–752.
42. Dinetz, S. F.; Bird, E. J.; Wagner, R. L.; Fountain, A. W. *J. Anal. Appl. Pyrol.* **2002**, *63*, 241–249.

43. Eigler, S.; Dotzer, C.; Hirsch, A.; Enzelberger, M.; Muller, P. *Chem. Mater.* **2012**, *24*, 1276–1282.

44. Feng, J.; Hao, J. W.; Du, J. X.; Yang, R. *J. Polym. Degrad. Stabil.* **2012**, *97*, 605–614.

45. Luftl, S.; Archodoulaki, V. M.; Seidler, S. *Polym. Degrad. Stabil.* **2006**, *91*, 464–471.

46. Popescu, C. *Thermochim. Acta* **1996**, *285*, 309–323.

47. Yang, M. H. *J. Appl. Polym. Sci.* **2002**, *86*, 1540–1548.

48. Li, X. G.; Huang, M. R. *Polym. Degrad. Stabil.* **1999**, *64*, 81–90.

49. Tomaszewicz, E.; Kotfica, M. *J. Therm. Anal. Calorim.* **2004**, *77*, 25–31.

50. Lua, A. C.; Su, J. C. *Polym. Degrad. Stabil.* **2006**, *91*, 144–153.

51. Lin, J. P.; Chang, C. Y.; Wu, C. H.; Shih, S. M. *Polym. Degrad. Stabil.* **1996**, *53*, 295–300.